Dominantly epitaxial growth of graphene on Ni (111) substrate

Zsolt Fogarassy[1], Mark H. Rümmeli[2,3], Sandeep Gorantla[4], Alicja Bachmatiuk[2,3,4], Gergely Dobrik[1], Katalin Kamarás[5], László Péter Biró[1], Károly Havancsák[6], János L. Lábár[1*]

[1] Hungarian Academy of Sciences, Research Centre for Natural Sciences, Institute for Technical Physics and Materials Science, Konkoly Thege M. út 29-33, H-1121 Budapest, Hungary

[2] IBS Center for Integrated Nanostructure Physics, Institute for Basic Science (IBS), Daejon 305-701, Republic of Korea

[3] Department of Energy Science, Department of Physics, Sungkyunkwan University, Suwon 440-746, Republic of Korea

[4] Leibniz Institute for Solid State Materials Research Dresden, Helmholtzstraße 20, 01069 Dresden, Germany

[5] Hungarian Academy of Sciences, Wigner Research Centre for Physics, Institute for Solid State Physics and Optics, Konkoly Thege M. út 29-33, H-1121 Budapest, Hungary

[6] Department of Materials Physics, Eötvös Loránd University, Pázmány Péter sétány 1/a., H-1117 Budapest, Hungary

Abstract

Graphene was grown on a Ni (111) thin layer, used as a substrate. The Ni layer itself was grown on single crystal sapphire (0001). Carbon was deposited by chemical vapor deposition using a mixture of methane, argon and hydrogen at atmospheric pressure implementing a constant gas flow (4.8-5 l/min) varying both the gas composition and the deposition temperature (900-980°C) and cooling rate (8-16°C/min) in the different experiments. Formation of uninterruptedly grown epitaxial single layer graphene was observed over the Ni (111) thin film substrate. Epitaxial growth was proven through STM measurements. Electron diffraction studies, also confirmed by STM, demonstrated that only one dominant orientation exists in the graphene, both results providing evidence of the epitaxial growth. On top of the, continuous, large area graphene flakes were also observed with sizes varying between 10 nm and 10 μm. Most of the top flakes are turbostratically related to the continuous underlying epitaxial graphene layer. The formation of the graphene layer with constant dominant orientation was observed over millimeter wide areas. Large areas (≈20-40 μm in

---

[*] Corresponding author. Tel: +36 1 392-26-92, e-mail: labar.janos@ttk.mta.hu (J.L. Lábár)

diameter) of continuous, epitaxial graphene, free of additional deposits and flakes were obtained for the best set of growth parameters.

1. Introduction

Both charge carrier mobility and thermal conductivity of graphene make it a promising candidate for becoming a future microelectronic material [1-6]. The best carrier mobility was measured in graphene that was prepared by mechanical exfoliation from graphite [7]. Unfortunately this method cannot be scaled up to industrial usage.

One of the most promising methods to produce graphene for electronic applications is chemical vapor deposition (CVD) on different metal substrates [8]. The most frequently used metal substrate is copper [9]. A big advantage of Cu against Ni or Co is that mainly single layer graphene grows on top of it because it has a very low solubility for carbon at high temperatures unlike nickel or cobalt. The graphene grown on copper may contain many grain boundaries (GB) [10], which reduce carrier mobility [11]. Consequently, it is not optimal for electronic applications. Another difficulty is that the melting point of the copper (1083°C) is near to the temperature of carbon deposition ($\approx$900°C) resulting in the development of a strong step structure during graphene growth [12-13]. The nano-wrinkles originating from this step structure will be present even after transfer of the grown graphene layer onto SiO_2 and will have a negative effect on electric transport [14].

Large area graphene can also be grown on single crystal nickel substrate with [111] orientation [15]. Nickel has a higher melting point (1453°C) than copper, but non-negligible amounts of carbon are dissolved into it at high deposition temperatures (>600°C). Dissolved carbon atoms precipitate on the surface of the substrate during the cooling period and they form graphene. If the nickel substrate contains grain boundaries, they act as a fast diffusion path and the precipitated carbon concentration is increased at the grain boundaries. A second layer of graphene or few layer graphite can also form at locations where the carbon concentration is too high (e.g. above the Ni grain boundaries) [15-17]. Therefore, a solution to this problem can be the use of single crystal nickel (sc-Ni) without GBs as a substrate to avoid inhomogeneous carbon precipitation and formation of concomitant carbon deposits [15, 18-21]. A very small lattice misfit (1.3%) exists between Ni [111] and graphene, so an epitaxial growth is anticipated and growth of graphene without GBs seems to be possible. The sc-Ni is expensive, so a possible economic solution is to grow a Ni [111] thin film on sc-MgO [18] or on sc-sapphire and use it as a substrate for the subsequent growth of graphene [22]. Graphene grown on Ni (111) contains only a few defects as shown by Raman studies [18, 22].

Low energy electron diffraction (LEED) examinations confirmed that graphene can grow epitaxially on Ni (111) below 600°C [18, 23, 24, 25, 26, 27]. The epitaxy breaks down above 600°C, the orientation of the layer rotated with 17° to the nickel becomes dominant and turbostratic carbon formed on the surface [24, 25, 28]. The authors of those publications did not explain the value of the observed rotation but concluded that epitaxy is not formed above 600°C substrate temperature. As a single exception, isolated triangular graphene domains were formed epitaxial on the Ni (111) substrate under extremely low growth rate at 925°C temperature, observed by in-situ LEEM and PEEM [29]. We show here that formation of epitaxial graphene is also possible at that high temperature even at usual growth rates.

Theoretical simulations of defect-free growth showed that the arriving carbon atoms have only one energetically favorable arrangement on the surface of Ni (111). That arrangement is called the Rosai structure (hollow site), and only that arrangement provides a global minimum in the interaction energy between the substrate surface and the graphene layer [30]. However, scanning tunneling microscopy (STM) studies demonstrated the presence of GBs in the graphene grown on Ni (111), which was attributed to the fact that monolayer NiC can form locally on the nickel surface and on that NiC the graphene will not grow epitaxially [21]. The presence of single layer thin NiC was only observed below 460°C [21, 31]. When deposition temperature exceeded 600°C only graphene was formed [18].

It is shown in this paper that (in contrast to previous studies) large areas of predominantly epitaxial graphene can be grown on thin Ni (111) film substrate even at higher temperatures (900-980°C). The Ni film itself was previously grown on sc-sapphire [32]. The atomic structure of the graphene and its orientation relationship with the nickel substrate were examined in detail.

2. Experimental methods

Graphene was deposited by CVD on a Ni (111) thin layer substrate, which had been prepared by sputtering Ni on sc-sapphire (0001) in ultrahigh vacuum (UHV) [32]. The thickness of the nickel layers were 375 nm. Twin boundaries were found in the nickel thin layers. Some of layers contain grains with 30° rotation. Location of these rotated areas might correspond to places where the sapphire might be dirty. In an effort to economize on materials costs polycrystalline nickel sputtered on SiO_2 at 550°C was also used as a cheap substrate at the early stage of the experiments for the optimization of the deposition parameters of the CVD process. The CVD experiments were performed in atmospheric pressure at a constant (4.8-5 l/min) flow of a mixture of argon, hydrogen and methane gases. Prior to the growth of

graphene, the nickel substrate was annealed in hydrogen at 900^oC temperature with 2 l/min gas flow. Deposition temperature was varied between 820-980^oC and cooling rate was varied between 8-16^oC/min for the different experiments. Composition of the gas mixture was also varied, as summarized in Table 1.

The graphene grown on nickel was examined with optical microscopy, Raman spectroscopy, atomic force microscopy (AFM), STM, with different transmission electron microscopes (TEM) (Philips CM20 operated at 200 keV and JEOL 2010 spherical aberration (C_s) corrected HRTEM operated at 80 keV [33]). Since additional flakes also appeared on top the single layer graphene, the orientation relation and locations of formation of the multilayer flakes were also studied with scanning electron microscopy (SEM) and electron backscattered diffraction (EBSD).

For the TEM studies the graphene was transferred from the nickel surface to a commercial holey amorphous carbon membrane on a gold TEM grid (commercial product of Quantifoil Micro Tools GmbH). The hole-size in the grid was 2 µm and the holes were separated 4 µm from each other. The transfer procedure started with dropping a drop of alcohol on the graphene surface then placing the TEM grid over it. Next, another drop of alcohol was dropped to the TEM grid and the sample was placed on an 180^oC hotplate to reach good sticking. When the alcohol evaporated, the holey amorphous carbon stuck to the graphene surface. After that the nickel was dissolved in $FeCl_3$ from under the graphene. When the Ni was dissolved completely, the sample was washed in distilled water and dried [34]. Fast evaporation of alcohol is important for good sticking. In that way it was possible to reach that almost the entire surface of the holey amorphous carbon stuck to the graphene surface.

An FEI Quanta 3D FEG scanning electron microscope was utilized for recording SEM images and backscattered electron diffraction (EBSD) patterns. For the EBSD measurements the sample was tilted to 70° as usual, with working distance of 12 mm and incoming electron energy of 20 keV. The EBSD Kikuchi patterns were detected using a high resolution Hikari camera. From the Kikuchi patterns an orientation map of the Ni layer was constructed.

Both the STM and AFM measurements were carried out with a Bruker MultiMode 8 microscope with Nanoscope V controller. The AFM data were acquired in tapping mode using Nanosensors SuperSharpSilicon tips (SSS-NCH-20), with 2 nm typical tip radius. The typical STM measurement parameters were 1 nA tunneling current and 100 mV bias voltage.

The Raman spectra were recorded using a Renishaw 1000 MB Raman microscope. The excitation source was the 488 nm line of an Ar^+ laser with incident power in the mW range in order to avoid excessive heating of the sample, using a laser spot with a diameter of 20 µm.

3. Results

Both types of our substrates (Ni (111), grown over sapphire and polycrystalline Ni, grown on SiO$_2$) were annealed in hydrogen prior to the carbon deposition to reduce surface oxidation. Additionally, the nickel grain size also increased with annealing. In the Ni (111) substrate layer, only two types of grain boundaries are present that determine the grain size. First, twin boundaries are observed. Second, occasionally the Ni grains are rotated with 30° degree around the surface normal and at these locations high energy grain boundaries are formed, however, the entire Ni film is epitaxial to the sapphire [0001] below it [32]. In case of the polycrystalline nickel thin layer substrate grown on SiO$_2$ the annealing increased the grain size to about 5-10 μm. Purging the chamber with Argon at room temperature is important to get rid of oxygen contamination. If oxygen is present, it can oxidize the nickel at the beginning of the annealing or can form Ni$_2$O$_3$ nanoparticles at the grain boundaries which could hinder the movement of grain boundary later. Example for the presence of such nanoparticles is shown in images from an oxygen-contaminated cross sectional TEM sample in figure 1. The oxide phase was identified with selected area electron diffraction (figure 1.b) and the composition of the phase was also confirmed with EDS. The appearance of such phases was also reported in the literature [35-36].

During cooling it is important to add hydrogen to the argon gas flow, because if only argon is used, a significant quantity of weakly bound carbon (most probably in amorphous form) remains deposited on the top of the nickel and graphene. The effect is illustrated for the case of the polycrystalline Ni substrate. Figure 2.a shows an optical image of a sample where no hydrogen was applied during the cooling, while figure 2.b shows an image of a sample where hydrogen was used during the cooling. Without hydrogen the surface is covered with excess carbon. When hydrogen was used the majority of the excess (most probably amorphous) carbon disappeared, only flakes of a second layer of graphene and/or graphite remained in reduced quantity above the nickel grain boundaries. Flakes surrounding a nickel grain are seen in the insert of figure 2.b. The reduced quantity of excess carbon is attributed to the effect of hydrogen. It was shown that the hydrogen annealing can reduce the amount of amorphous carbon on the substrate surface. The hydrogen can act both as a reducing reagent and a carrier gas to remove C atoms [37].

Figure 3 shows the optical images of samples grown on Ni (111) substrate with different growth parameters, reported in Table 1. Single layer graphene was continuously grown on large area on all samples according to the STM, TEM and Raman investigations and the

continuous single layer was covered with different amounts of flakes of graphene and graphite. The AFM studies showed that these flakes are above the continuously grown single layer graphene and they are not situated between the nickel and the graphene (figure 4). If the flakes would be situated underneath the grown graphene, like it was recently reported for a Cu island on Cu (111) formed underneath the graphene layer [38], the slope of the AFM profile at the edges of the flakes would be smaller as reported for example for Au islands under graphene (see Fig. 1.c in [39]). Moreover, a linecut taken through a small enough size hollow between the islands - over which the graphene would be suspended, if the islands would be situated underneath the graphene layer - clearly shows that this is not the case (Fig. 4). The islands are formed on the top of the continuous graphene layer. The larger fraction of the flakes are turbostratically positioned on the single layer graphene as observed from TEM investigations in figure 5. Nevertheless, flakes with the same orientation as the continuous graphene were also found, which is presumably AB staking as shown in figure 6, where the orientation of a 0.5 μm wide flake was found to be the same as the orientation of the neighboring large area single layer graphene.

Both the coverage (%) of the coherent graphene by the flakes and the flake density (pieces/μm^2) are shown in the last two columns of table 1 as measured from the optical microscope image. When the hydrogen gas flow was reduced during the deposition smaller flakes appeared next to the larger ones. With increasing the methane gas flow to triple amount during the deposition, the larger flakes became thicker and additional smaller flakes appeared. Four times increase of the deposition time did not change much the average distribution and the size of the flakes, but the chain of flakes became contiguous above the 30° grain boundaries or incoherent twin boundaries in the nickel substrate, as shown by the SEM image and the EBSD orientation map in figure 7. When the deposition temperature was decreased from 980^oC to 900^oC with the higher hydrogen gas flow the smaller flakes disappeared and the size of the remaining flakes doubled, so the continuous single layer graphene became free from flakes in large areas. A different behavior was observed when hydrogen flow was reduced during deposition at the same temperature. The size of the flakes was reduced to 1/2 or ¼ of that of the flakes grown at higher temperature with the same hydrogen flow.

An increase in the cooling time did not change either the density or the size of the flakes significantly, but the flakes became thinner.

The largest area (≈20-40 μm in diameter) without flakes was formed on the sample prepared with high hydrogen flow (3.8 l/min) at 900°C. The STM image taken on that sample is shown in figure 8. The graphene atomic lattice is visible in the higher magnification STM images.

The nickel atomic steps are seen that correspond to the line traces of other nickel (111) planes (the surface line-traces of dislocations moving on the glide planes of nickel). In the smaller magnification STM images the manually drawn dark lines mark the graphene zigzag edges, which were determined by the atomic resolution images taken on the same location of the sample. The large scale STM images are more strongly affected by drift due to the lower scan speed used to allow the STM tip to follow the relief of the surface without colliding with it than the atomic resolution images acquired at higher scan speeds. The large scale images were drift corrected using the angles between the Ni step edges. As the step edges should make 60° with each other, the as recorded STM images were modified to exhibit these angles. On the drift corrected STM images the orientation of the zigzag directions extracted from the atomic resolution STM images precisely matches the orientation of the Ni steps. The nickel (111) planes are parallel to the zigzag edges of graphene according to our observations in several areas. No different orientation relationships or grain boundaries were found in the graphene by STM. The orientation of the top atomic layer of the nickel did not change when a twin boundary is crossed. Consequently, the graphene orientation did not change either. Above the occasionally found 30° boundaries the graphene can change orientation.

Only one dominant orientation of the graphene was found by TEM by sampling several flake-free areas far (10 μm-1 mm away) from each other. This fact is interpreted as the graphene extending over about 1 mm wide area follows epitaxially the substrate surface structure. Selected area electron diffraction patterns from such areas are shown in Figure 9. In addition to the spots of the dominant orientation, additional smeared small spots also appeared that must originate from smaller grains. The graphene with dominant orientation is about 2/3 part of the total area, based on the relative intensity of its diffraction spots in the SAED images.

These smaller grains were also found in the HRTEM images recorded from the single layer graphene. A grain boundary between the large dominant orientation and a small grain is shown in Figure 10.a, where the two orientations are rotated with respect to each other by 25° degrees. STM study of this same sample was difficult. This sample was densely covered with turbostratically oriented flakes of 10-20 μm size, as shown by the Moiré pattern in the TEM image of Figure 10.b. That is why only the samples, cleaner from flakes were only examined by STM.

Raman investigations were performed on graphene layers transferred to TEM grids, because the Raman spectrometer is not able to detect graphene on top of nickel. The Raman studies were done on samples with low flake density, where the flake-free areas are larger than the area sampled by Raman (the laser spot was 20 μm). It was straightforward to obtain a

spectrum of pure graphene from the spectra recorded on the sample with low flake density (figure 3, sample 6). Since the transferred graphene was inseparable from an amorphous carbon support film, the effect of this support film had to be removed. First the Raman spectrum was recorded on an average area where the graphene was situated above the amorphous support film and the spectrum also contained the contribution from the amorphous support film. The contribution of the amorphous background from the Quantifoil carbon membrane was measured separately in a graphene-free region and was subtracted from the first spectrum. The Raman spectra are shown in figure 11.

It is seen from the Raman spectrum recorded from the sample with low flake density that the graphene is single or bi-layer, evidenced by the ratio of the G peak to the 2D peak and by the shape of 2D peak [40]. The D peak corresponds to defects in graphene. Our experimental setup is similar to the setup when free standing graphene is measured: about half of the area illuminated by the Raman laser was above a hole in the holey carbon membrane and thus directly comparable to freestanding graphene samples. In exfoliated graphene under similar conditions, no D peak was detected [41]. The very small D peak in our Raman spectrum as compared to the free-standing-graphene grown on copper with CVD [42] suggests that only a few defects are present in our graphene layer. These defects can correspond to the grain boundaries of the few small grains in the graphene found by our HRTEM investigations (figure 10.a).

4. Discussion

The use of hydrogen during the cooling period removes the loosely bound (probably amorphous) carbon from the surface. The hydrogen can have two effects during cooling. First, it presumably accelerates the cooling due to its higher thermal conductivity. However, merely an increased cooling rate did not result in a disappearance of or reduction in the quantity of the amorphous carbon. Even more important effect of hydrogen is that it creates chemical bonds with the weakly bonded carbon atoms and forms methane, so it can take the carbon away from the sample surface. 5% hydrogen was used in the cooling gas because introduction of more hydrogen (25%) did not change significantly either the density or the size of flakes. The effect of hydrogen flow is more complex during deposition [43].

Nickel is a good catalyst, so the methane can decompose on its surface. After decomposition the freed-up carbon can dissolve into the nickel, or can desorb again [37, 44], or may remain on the surface and start to form graphene. In the entire examined parameter range the formation of continuous, large area single layer graphene was observed. Between the nickel

and the graphene there is a stronger interaction than between two graphene layers [21, 45]. Epitaxial growth of graphene on the Ni (111) is not against expectations, since there is good registry between graphene and the Ni (111) lattice. Additionally, the attraction between graphene and Ni is stronger than between two graphene layers. In contrast to that, the flakes can grow turbostratically on top of the coherently grown graphene. The graphene forms directly on the nickel before the flakes start to grow. For the flakes to be formed above the graphene the carbon atoms have to diffuse through the graphene and that diffusion is usually very slow if the graphene is perfect [46-47]. Consequently, diffusion can mainly happen through grain boundaries or at other defected locations in the graphene layer. However, certain metals (Pt, Pd, Au, Ni and Co) which were evaporated on graphene can diffuse through the graphene layer grown on SiC or Ru (111) even if the graphene is perfect, as it was shown in the literature [48-49]. That penetration is possible because the metal can get to an energetically more favorable position between the graphene and the substrate than it has on top of the graphene [48-49]. However, carbon behaves differently from those metals and it is not accumulating between the graphene and the nickel. On the contrary, it segregates on the free surface of the graphene, opening the way to the formation of the flakes and the amorphous patches on top of the graphene. Our AFM observations are interesting, because they are different from the results detected by others. On the basis of LEED-based literature, the second graphene layer formed between the substrate and the first continuous layer of graphene in the case of Cu [50], Ir (111) [51] and Ni (111) substrates [52]. The case of the Cu substrate differs from the Ni substrate, because the Cu does not dissolve the carbon, unlike Ni, so other mechanisms dominate in the formation of the bilayer graphene in case of Cu. Ir is more similar to Ni because it can dissolve carbon. However, the LEED pattern [52] recorded on graphene covered Ni (111) is different from what we observed during the formation of our graphite patches. During the growth of the second layer [52] a dendritic formation takes place, because the strong Ni-graphene bonds have to be broken during the growth of the second layer, as those authors assume, and before the 3rd layer forms the second layer covers the surface of the substrate [52]. Their different observation does not contradict ours, because the growth parameters are different in our case (i.e. they deposited the carbon in vacuum and they didn't mention the use of hydrogen). Growth of carbon on the nickel (111) surface resembles the Stranski-Krastanow (S-K) growth mode [53]. The S-K growth mode starts with a 2D grow, in our case a single layer graphene is formed on the top of the nickel substrate, later it turns into a 3D growth, where three dimensional multilayer islands are formed [54-55]. The main driving force for the 2D growth is the good wetting between the Ni (111) and the graphene.

The first continuous layer stores elastic energy due to the misfit. In order to moderate the increase of the stored elastic energy with the increasing number of layers the subsequently nucleated layers grow in islands which results in a 3D growth.

The nickel dissolves carbon well at the deposition temperature ($\geq 900°C$). The quantity of the dissolved carbon depends on the experimental parameters used during the deposition (temperature, hydrogen and methane gas flow, deposition time). The presence of carbon on the surface of nickel can slow down the decomposition of methane, so the dissolution rate of carbon into Ni not only limits the quantity of carbon dissolved in the Ni substrate but also controls the quantity of the adsorbed free carbon on the surface of Ni. Since grain boundaries manifest a fast diffusion path, these locations both store more carbon during deposition and emit more carbon during the cooling period. After a longer deposition time it is seen that the size of the flakes increases above the defects in the nickel substrate, especially above high energy (30°) grain boundaries and incoherent twin boundaries, as evidenced by our EBSD studies. It is interpreted as the consequence of enhanced local emission of carbon above areas where the diffusion is faster than in the bulk substrate. According to the literature, the diffusion of copper in nickel is 2.5 times higher through twin boundaries than in the bulk [56]. We assume that diffusion of the smaller carbon atoms must also be enhanced similarly through incoherent twin boundaries, since the atomic radius of carbon is 70 pm, while that of copper is 135 pm. No similar enrichment in carbon has been observed above coherent twin boundaries in the Ni substrate. The larger flakes are formed above incoherent twin boundaries of the substrate.

When the cooling velocity was decreased neither the flake size nor the flake density did change significantly but the flakes became thinner (figure 3, sample 2). The flakes grow thinner, because at a slower cooling the hydrogen has more time to take away the unbound carbon atoms from the top of the flakes before they can reach enough quantity to nucleate a new atomic layer and thicken the flake.

The higher methane flow rate during deposition also results in a smaller number of larger and thinner flakes (figure 3, sample 5). The carbon concentration on the surface will be uniformly higher during deposition with the relative increase of methane (and the concomitant relative decrease of the hydrogen), because the carbon will re-form into methane with smaller probability on the nickel surface and that larger amount of carbon is solved in the Ni substrate. During the cooling period precipitation of that higher amount of dissolved carbon will result in higher average carbon concentration on the surface and it will start to nucleate flakes in

more points and as a consequence of the increased nucleation density, smaller flakes will be formed. However, the larger number of small flakes results in a larger coverage (Table 1). Decreasing the deposition temperature to 900°C has double effect when the hydrogen flow is kept at the lower rate (1.7 l/min). At lower temperature both the catalytic efficiency of the nickel is reduced and the diffusion is decreased, so lower amount of carbon is dissolved into the Ni substrate. In addition to that, the surface diffusion will also be slower at the beginning of the cooling period (as compared to the case when cooling starts from higher temperature) and the carbon mobility will also be lower on the surface. So, the nucleation starts in more points and the flakes grow smaller but their density will be higher [57], as shown by comparing sample 4 (980°C) and sample 7 (900°C) in figure 3. The opposite effect can be observed by lowering the temperature while the hydrogen gas flow is higher (3.7 l/min) during the deposition (compare sample 3 (980°C) and sample 6 (900°C) in figure 3). In this case the flakes are larger at lower temperature than in the case of the sample deposited with the same high hydrogen gas flow at higher temperature. This can be understood because that carbon concentration can reach the critical concentration needed for nucleation only above grain boundaries or incoherent twin boundaries due to the larger hydrogen flow, but these flakes can collect carbon atoms from a larger area, because there are no smaller flakes between them and, due to that the number density of flakes is much smaller.

5. Conclusions

Presumably, at the temperatures used during deposition (≥900°C) carbon is dissolved into the nickel substrate. During cooling the dissolved carbon precipitates and single layer graphene is formed predominantly epitaxially and continuously on the Ni (111) surface. Next, either another layer of graphene or graphite flakes can be formed on top of the continuously grown large area, single layer graphene with random orientation relationship. The size and density of flakes are determined by the quantity and distribution of the precipitated carbon. In the case of a polycrystalline nickel substrate (figure 2) growth of both the graphene and the flakes starts above the grain boundaries in the nickel substrate. In contrast to that, formation of the graphene is relatively homogeneous on a Ni (111) substrate. However, larger flakes were also observed to grow above the high energy (30°) grain boundaries and above the incoherent twin boundaries of the substrate (figure 3). The best graphene can be grown when the Ni substrate does not have high energy boundaries (between Ni grains rotated by 30° from each other). That Ni (111) substrate only contains twin boundaries. Since diffusion through coherent twin boundaries is similar to that in bulk nickel, the carbon distribution is close to homogeneous

above them. The presence of incoherent twin boundaries can still remain a problem as they act as enhanced local carbon sources and their elimination requires further effort. It is hard to control the quantity of the carbon dissolved into the Ni and consequently of the precipitated carbon, however, the use of hydrogen under the cooling process can take away the loosely bound extra carbon by forming hydrocarbons like methane that desorbs. In that way large areas (≈20-40 μm in diameter) of single layer graphene, free of deposits or flakes can be produced.

References

[1] K.S. Novoselov, A.K. Geim, S.V. Morozov, D. Jiang, Y. Zhang, S.V. Dubonos, I.V.Grigorieva, A.A. Firsov, Electric Field Effect in Atomically Thin Carbon Films, Science 306 (2004) 666-669.

[2] K.S. Novoselov, D. Jiang, F. Schedin, T.J. Booth, V.V. Khotkevich, S.V. Morozov, and A.K. Geim, Two-dimensional atomic crystals, PNAS 102 (2005) 10451-10453.

[3] A.K. Geim, K.S. Novoselov, The rise of graphene. Nature materials 6 (2007) 183-191.

[4] A.K. Geim, Graphene: Status and Prospects, Science 324 (2009) 1530-1534.

[5] M.J. Allen, V.C. Tung, R.B. Kaner, Honeycomb Carbon: A Review of Graphene, Chem. Rev. 110 (2010) 132–145.

[6] M.H. Rümmeli, C.G. Rocha, F.Ortmann, I.Ibrahim, H.Sevincli, F.Börrnert, J.Kunstmann, A.Bachmatiuk, M.Pötschke, M.Shiraishi, M.Meyyappan, B.Büchner, S.Roche, G.Cuniberti, Graphene: Piecing it Together, Advanced Materials 23 (2011) 4471–4490.

[7] K.I. Bolotin, K.J. Sikes, Z. Jiang, M. Klima, G. Fudenberg, J. Hone, P. Kim, H.L. Stormer, Ultrahigh electron mobility in suspended graphene, Solid State Communications 146 (2008) 351–355.

[8] C. Mattevi, H. Kim, M. Chhowalla, A review of chemical vapour deposition of graphene on copper, J. Mater. Chem. 21 (2011) 3324-3334.

[9] X. Li, C.W. Magnuson, A. Venugopal, J. An, J. W. Suk, B. Han, M. Borysiak, W. Cai, A. Velamakanni, Y. Zhu, L. Fu, E. M. Vogel, E. Voelkl, L. Colombo, R.S. Ruoff, Graphene Films with Large Domain Size by a Two-Step Chemical Vapor Deposition Process, Nano Lett. 10 (2010) 4328–4334.

[10] L.P. Biró, P. Lambin, Grain boundaries in graphene grown by chemical vapor deposition, New Journal of Physics 15 (2013) 035024.

[11] Q. Yu, L.A. Jauregui, W. Wu, R. Colby, J. Tian, Z. Su, H. Cao, Z. Liu, D. Pandey, D. Wei, T.F. Chung, P. Peng, N.P. Guisinger, E. A. Stach, J. Bao, S.S. Pei, Y.P. Chen, Control and characterization of individual grains and grain boundaries in graphene grown by chemical vapour deposition, Nature Materials 10 (2011) 443-449.

[12] J.M. Wofford, S. Nie, K.F. McCarty, N.C. Bartelt, O.D. Dubon, Graphene Islands on Cu Foils: The Interplay between Shape, Orientation, and Defects, Nano Lett. 10 (2010) 4890–4896.

[13] K. Kertész, A.A. Koós, A.T. Murdock, Z. Vértesy, P. Nemes-Incze, P.J. Szabó, Z.E. Horváth, L. Tapasztó, Chanyong Hwang, N. Grobert, and L. P. Biró, Polarized light microscopy of chemical-vapor-deposition-grown graphene on copper, Applied Physics Letters 100 (2012) 213103-213103-5.

[14] G.X. Ni, Y. Zheng, S. Bae, H.R. Kim, A. Pachoud, Y.S. Kim, C.L. Tan, D. Im, J.H. Ahn, B.H. Hong, B. Ozyilmaz, Quasi-Periodic Nanoripples in Graphene Grown by Chemical Vapor Deposition and Its Impact on Charge Transport, ACS Nano. 6 (2012) 1158-64.

[15] Y. Zhang, L. Gomez, F.N. Ishikawa, A. Madaria, K. Ryu, C. Wang, A. Badmaev, C. Zhou, Comparison of Graphene Growth on Single-Crystalline and Polycrystalline Ni by Chemical Vapor Deposition, J. Phys. Chem. Lett. 1 (2010) 3101-3107.

[16] A. Reina, X. Jia, J. Ho, D. Nezich, H. Son, V. Bulovic, M.S. Dresselhaus, J. Kong, Layer area, few-layer graphene films on arbitrary substrates by chemical vapor deposition, Nano Lett. 9 (2009) 30-35.

[17] A. Reina, S. Thiele, X. Jia, S. Bhaviripudi, M.S. Dresselhaus, J.A. Schaefer, J. Kong, Growth of large-area single- and Bi-layer graphene by controlled carbon precipitation on polycrystalline Ni surfaces, Nano Res 2 (2009) 509-516.

[18] T. Iwasaki, H.J. Park, M. Konuma, D.S. Lee, J.H. Smet, U. Starke, Long-Range Ordered Single-Crystal Graphene on High-Quality Heteroepitaxial Ni Thin Films Grown on MgO(111), Nano Lett. 11 (2011) 79-84.

[19] C.M. Orofeo, H. Ago, B. Hu, M. Tsuji, Synthesis of large area, homogeneous, single layer graphene films by annealing amorphous carbon on Co and Ni, Nano Res. 4 (2011) 531-540.

[20] H. Ago, I. Tanaka, C.M. Orofeo, M. Tsuji, K. Ikeda, Patterned Growth of Graphene over Epitaxial Catalyst. Small 6 (2010) 1226-1233.

[21] P. Jacobson, B. Stöger, A. Garhofer, G.S. Parkinson, M. Schmid, R. Caudillo, F. Mittendorfer, J. Redinger, U. Diebold, Nickel Carbide as a Source of Grain Rotation in Epitaxial Graphene, ACSNano 6 (2012) 3564–3572.

[22] S. Yoshii, K. Nozawa, K. Toyoda, N. Matsukawa, A. Odagawa, A. Tsujimura, Suppression of Inhomogeneous Segregation in Graphene Growth on Epitaxial Metal Films, Nano Lett. 11 (2011) 2628-2633.

[23] Y. Gamo, A. Nagashima, M. Wakabayashi, M. Terai, C. Oshima, Atomic structure of monolayer graphite formed on Ni(111), Surface Science 374 (1997) 61-64.

[24] A. Dahal, R. Addou, P. Sutter, M. Batzill, Monolayer graphene growth on Ni(111) by low temperature chemical vapor deposition, APPLIED PHYSICS LETTERS 100 (2012) 241602.

[25] L. L. Patera, C. Africh, R. S. Weatherup, R. Blume, S. Bhardwaj, C. Castellarin-Cudia, A. Knop-Gericke, R. Schloegl, G. Comelli, S. Hofmann, C. Cepek, In Situ Observations of

the Atomistic Mechanisms of Ni Catalyzed Low Temperature Graphene Growth, ACSNano 7 (2013) 7901.

[26] M. Xu, D. Fujita, K. Sagisaka, E. Watanabe, and N. Hanagata, Production of extended single-layer graphene. ACSNano 5 (2011) 1522.

[27] R. Addou, A. Dahal, P. Sutter, M. Batzill, Monolayer graphene growth on Ni(111) by low temperature chemical vapor deposition. APPLIED PHYSICS LETTERS 100 (2012) 021601.

[28] A. Dahal, H. Coy-Diaz, R. Addou, J. Lallo, E. Sutter, M. Batzill, Preparation and characterization of Ni(111)/graphene/Y2O3(111) heterostructures, JOURNAL OF APPLIED PHYSICS 113 (2013) 194305.

[29] M. Li, J.B. Hannon, R.M. Tromp, J. Sun, J. Li, V.B. Shenoy, E. Chason, Equilibrium shape of graphene domains on Ni(111), PHYSICAL REVIEW B 88 (2013) 041402.

[30] Y. Shibuta, J. A.Elliott, Interaction between graphene and nickel(1 1 1) surfaces with commensurate and incommensurate orientational relationships, Chemical Physics Letters 538 (2012) 112-117.

[31] J. Lahiri, T. Miller, L. Adamska, I.I. Oleynik, M. Batzill, Graphene Growth on Ni(111) by Transformation of a Surface Carbide, Nano Lett. 11 (2011) 518–522.

[32] Z. Fogarassy, G. Dobrik, L.K. Varga, L.P. Biró, J.L. Lábár, Growth of Ni layers on single crystal sapphire substrates, Thin Solid Films 539 (2013)96-101.

[33] F. Boerrnert, A. Bachmatiuk, S. Gorantla, D. Wolf, A. Lubk, B. Buechner, M.H. Rummeli, Retro-fitting an older (S)TEM with two Cs aberration correctors for 80 kV and 60 kV operation, Journal of Microscopy 249 (2013) 87-92.

[34] W. Regan, N. Alem, B. Alemán, B. Geng, Ç. Girit, L. Maserati, F. Wang, M. Crommie, A. Zettl, A direct transfer of layer-area graphene, App. Phys. Letters 96 (2010) 113102.

[35] P.S. Aggarwal, A. Goswami, AN OXIDE OF TERVALENT NICKEL, J. Phys. Chem. 65 (1961) 2105-2105.

[36] J. Kang, S. Rhee, Chemical vapor deposition of nickel oxide films from Ni(C5H5)2/O2, Thin Solid Films 391 (2001), 57-61.

[37] Z. Sun, Z. Yan, J. Yao, E. Beitler, Y. Zhu, J.M. Tour, Growth of graphene from solid carbon sources, Nature 468 (2010) 549–552.

[38] L. Tapasztó, T. Dumitrică, S.J. Kim, P. Nemes-Incze, C. Hwang, L.P. Biró, Breakdown of continuum mechanics for nanometre-wavelength rippling of graphene, Nature Physics 8 (2012) 739–742.

[39] S. Heeg, R. Fernandez-Garcia, A. Oikonomou, F. Schedin, R. Narula, S.A. Maier, A. Vijayaraghavan and S. Reich, Polarized Plasmonic Enhancement by Au Nanostructures Probed through Raman Scattering of Suspended Graphene, Nano Lett. 13 (2013) 301−308.

[40] A.C. Ferrari, J.C. Meyer, V. Scardaci, C. Casiraghi, M. Lazzeri, F. Mauri, S. Piscanec, D. Jiang, K.S. Novoselov, S. Roth, A.K. Geim, Raman Spectrum of Graphene and Graphene Layers, Phys. Rev. Lett. 97 (2006) 187401-187401-4.

[41] S. Berciaud, S. Ryu, L.E. Brus, T.F. Heinz, Probing the Intrinsic Properties of Exfoliated Graphene: Raman Spectroscopy of Free-Standing Monolayers, Nano Letters 9 (2009) 346-352.

[42] Y. Lin, C. Lu, C. Yeh, C. Jin, K. Suenaga, P. Chiu, Graphene Annealing: How Clean Can It Be?, Nano Lett. 12 (2012) 414−419.

[43] M. Losurdo, M.M. Giangregorio, P. Capezzuto, G. Bruno, Graphene CVD growth on copper and nickel: role of hydrogen in kinetics and structure, Phys. Chem. Chem. Phys. 13 (2011) 20836–20843.

[44] H. Mehdipour, K. Ostrikov, Kinetics of Low-Pressure, Low-Temperature Graphene Growth: Toward Single-Layer, Single-Crystalline Structure, ACSNano 6 (2012) 10276–10286.

[45] R. Zhao, Y. Zhang, T. Gao, Y. Gao, N. Liu, L. Fu, Z. Liu, Scanning tunneling microscope observations of non-AB stacking of graphene on Ni films, Nano Res. 4 (2011) 712–721.

[46] J. S. Bunch, S.S. Verbridge, J.S. Alden, A.M. van der Zande, J.M. Parpia, H.G. Craighead, P.L. McEuen, Nano Let. 8 (2008) 2458-2462.

[47] D. Jiang, V.R. Cooper, S. Dai, Porous Graphene as the Ultimate Membrane for Gas Separation, Nano Let. 9 (2009) 4019-4024.

[48] I. Gierz, T. Suzuki, R.T. Weitz, D.S. Lee, B. Krauss, C. Riedl, U. Starke, H. Höchst, J.H. Smet, C.R. Ast, K. Kern, Electronic decoupling of an epitaxial graphene monolayer by gold intercalation, Physical Reveiw B 81 (2010) 235408-235408-6.

[49] L. Huang, Y. Pan, L. Pan, M. Gao, W. Xu, Y. Que, H. Zhou, Y. Wang, S. Du, H.J. Gao, Intercalation of metal islands and films at the interface of epitaxially grown graphene and Ru(0001) surfaces, Appl.Phys.Let. 99 (2011) 163107-163107-3.

[50] S. Nie, W. Wu, S. Xing, Q. Yu, J. Bao, S. Pei, K.F McCarty, Growth from below: bilayer graphene on copper by chemical vapor deposition, New Journal of Physics 14 (2012) 093028.

[51] S. Nie, A.L. Walter, N.C. Bartelt, E. Starodub, A. Bostwick, E. Rotenberg, K.F. McCarty, Growth from Below: Graphene Bilayers on Ir(111). ACSNano 5 (2011) 2298.

[52] G. Odahara, S. Otani, C. Oshima, M. Suzuki, T. Yasue, T. Koshikawa, In-situ observation of graphene growth on Ni (111). Surface Science 605 (2011) 1095.

[53] I. N. Stranski, V.L. Krastanow, Akad. Wiss. Lit. Mainz Math.-Natur. Kl. IIb 146 (1939) 797.

[54] K. Shiramine, T. Itoh, S. Muto, T. Kozaki, S. Sato, Adatom migration in Stranski−Krastanow growth of InAs quantum dots, Journal of Crystal Growth 242 (2002) 332–338.

[55] D.J. Eaglesham, M. Cerullo, Dislocation-free Stranski-Krastanow growth of Ge on Si(100), Phys. Rev. Let. 64 (1990) 1943-1946.

[56] H. Helfmeier, M. Feller-Knjepmeier, Diffusion of Copper in Nickel Single Crystals, J. Appl. Phys. 41 (1970) 3202-3205.

[57] J. Zhou, Y.C. Kang, D.A. Chen, Controlling island size distributions: a comparison of nickel and copper growth on TiO2 (110), Surface Science 537 (2003) L429–L434.

Figure captions

Table 1. Growth parameters together with the coverage and density of the grown flakes for the different samples.

Sample	Deposition					Cooling rate [^{o}C/min]	Flakes	
	Temp. [^{o}C]	H$_2$ [l/min.]	Ar [l/min]	CH$_4$ [l/min]	Time [s]		Coverage [%]	Density [pc/μm^2]
1	980	3,7	1	0,1	1200	16	39	0,035
2	980	3,7	1	0,1	300	8	38	0,033
3	980	3,7	1	0,1	300	16	28	0,0439
4	980	1,7	3	0,1	300	16	41	0,0555
5	980	1,7	3	0,3	300	16	ca 70	ca 0,145
6	900	3,7	1	0,1	300	16	12	0,00227
7	900	1,7	3	0,1	300	16	ca 80	ca 0,36

Figure 1. Ni$_2$O$_3$ nanoparticles are seen in the bright field image a). The glue ripped off the particles from the nickel surface. Selected area diffraction b) was taken from the same area as the bright field image in a).
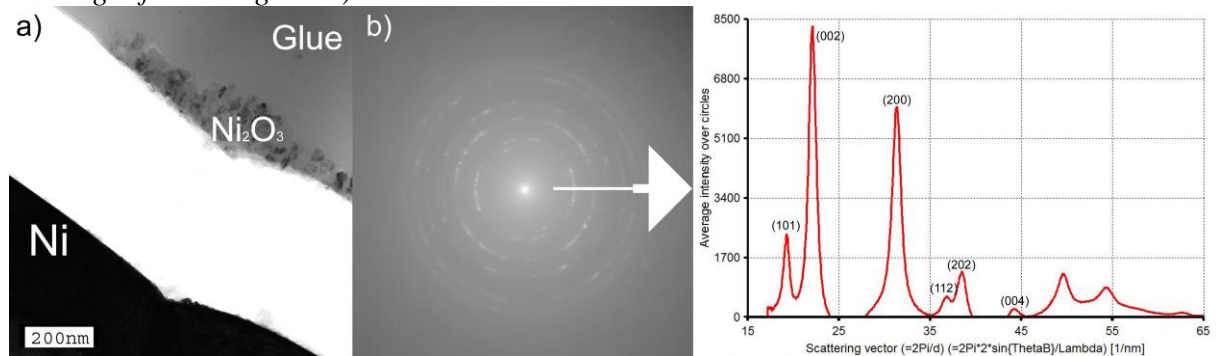
Figure 2. Optical images of carbon grown on polycrystalline nickel substrate are shown under two conditions. a) No hydrogen was used during the cooling period. Large amount of amorphous carbon and graphite flakes were formed on the graphene. b) Due to the use of hydrogen flow during the cooling period no amorphous carbon was formed. The remaining flakes started to grow above the nickel grain boundaries. The insert in b) shows flakes surrounding a nickel grain. The contrast variation of the different flakes comes from differences in thickness.
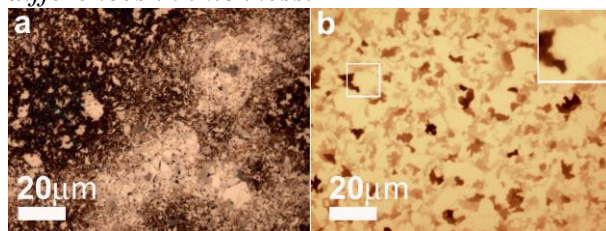

17

Figure 3. Optical images of the samples grown with different parameters. The darker patches are the graphene and/or graphite flakes. The lighter areas on the images, i.e. the background correspond to the single layer graphene on top of the Ni (111) substrate. The labels and the arrows indicate changes in deposition temperature, deposition time, flow rate of hydrogen and methane during deposition and cooling rate. The hydrogen flow rate during the cooling period was the same in all of these experiments. The figures are labeled with the sample numbers corresponding to table 1. Deposition parameters of the samples are given in table 1.
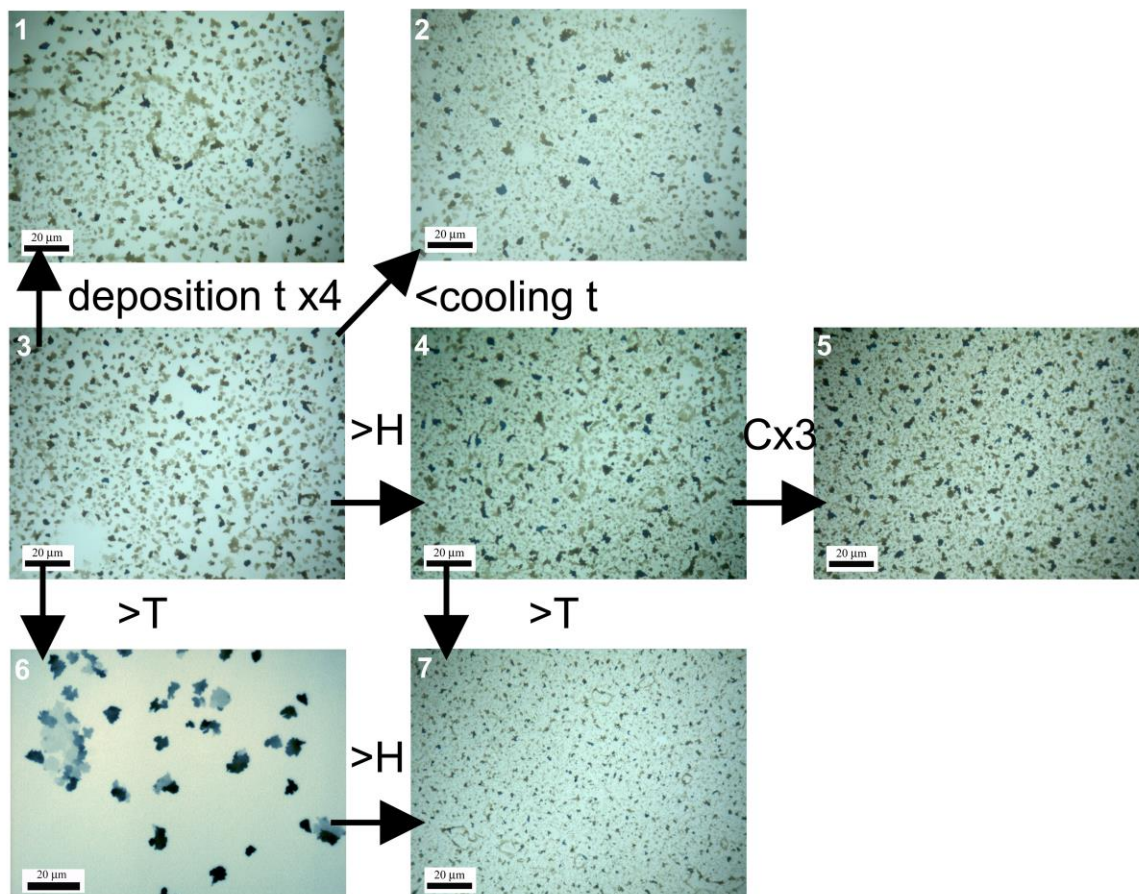
Figure 4. AFM image of the grown flakes. The flakes are above the continuous graphene as evidenced by their height. The line cut shows the thickness of the flakes.
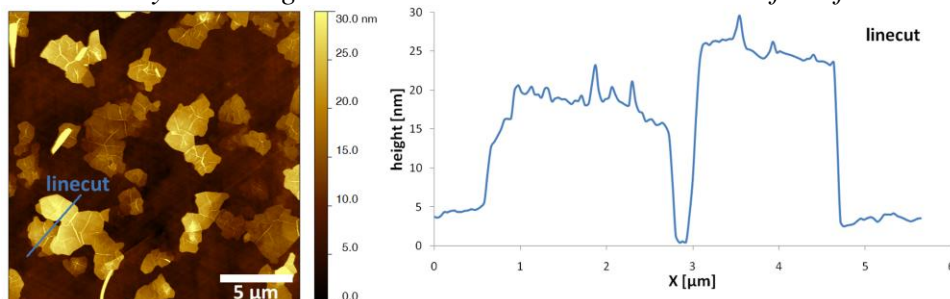
Figure 5. Bright field TEM image of a 4 µm size flake (on the left). The selected area diffraction on the right was taken from the area marked with the white circle on the left. The full arrows on the diffraction show the reflections from the flake, the empty arrows point to the spots coming from the graphene that was continuously grown on the Ni (111) substrate. The flakes are turbostratically grown on the continuous graphene since the reflections from the flake and the reflections from the continuous graphene are rotated relative to each other.
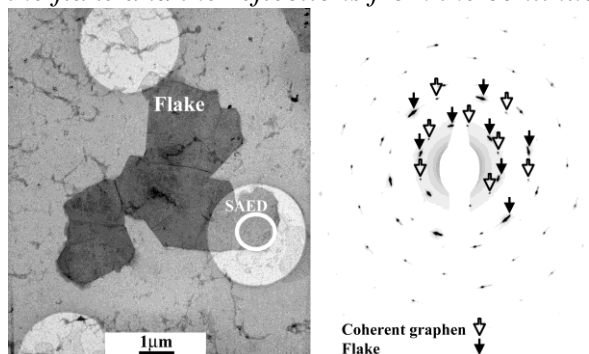
Figure 6. TEM image from the large area graphene and a flake over it. At the circled region "area1" no large flakes are present, while at "area2" one larger flake is also present on top of the continuous graphene layer. The reflections in the diffraction from "area1" and "area2" are in the same position, demonstrating that the flake is not rotated, so it is in AB stacking over the large area graphene. The dark patches over the graphene are solvent residues (contamination) which were created during the transfer process.
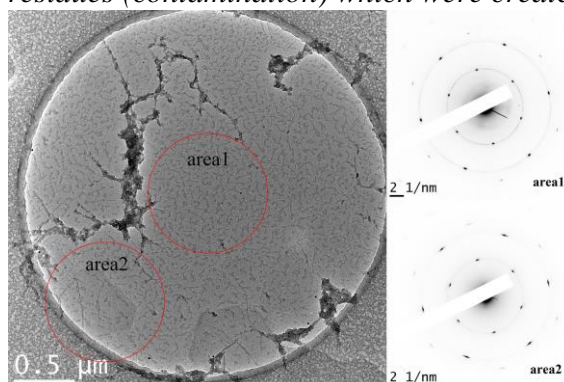

Figure 7. A sample with non-optimum deposition conditions and with 30°-boundary in the Ni was selected to study at which locations the flakes form. On this sample a large amount of flakes were observed, so it was possible to observe the relationship between the nickel substrate and both the thinner and the ticker flakes. On the left an SEM image of nickel surface with the flakes is shown. On the right an EBSD map is seen, recorded from the same area. On the SEM image the red lines mark twin boundaries. The arrows point to incoherent twin boundary sections where thicker flakes are formed. A 30° degree boundary is visible in the middle of the image. At this type of boundaries the flakes touch each other.
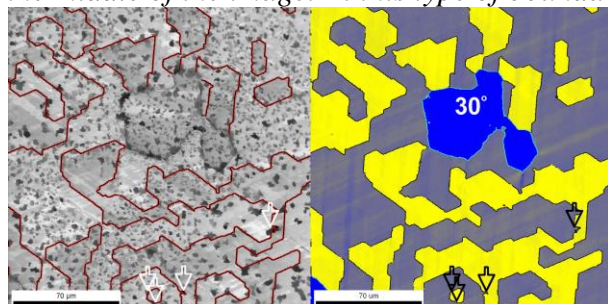
Figure 8. STM images of graphene. On the left (a, c images) the nickel atomic steps are visible in smaller magnification. On the right (b, d images) the graphene atomic lattice is shown in higher magnification images. In the smaller magnification images the manually drawn dark lines mark the graphene zigzag direction. The two pairs of images are taken from two similar areas.
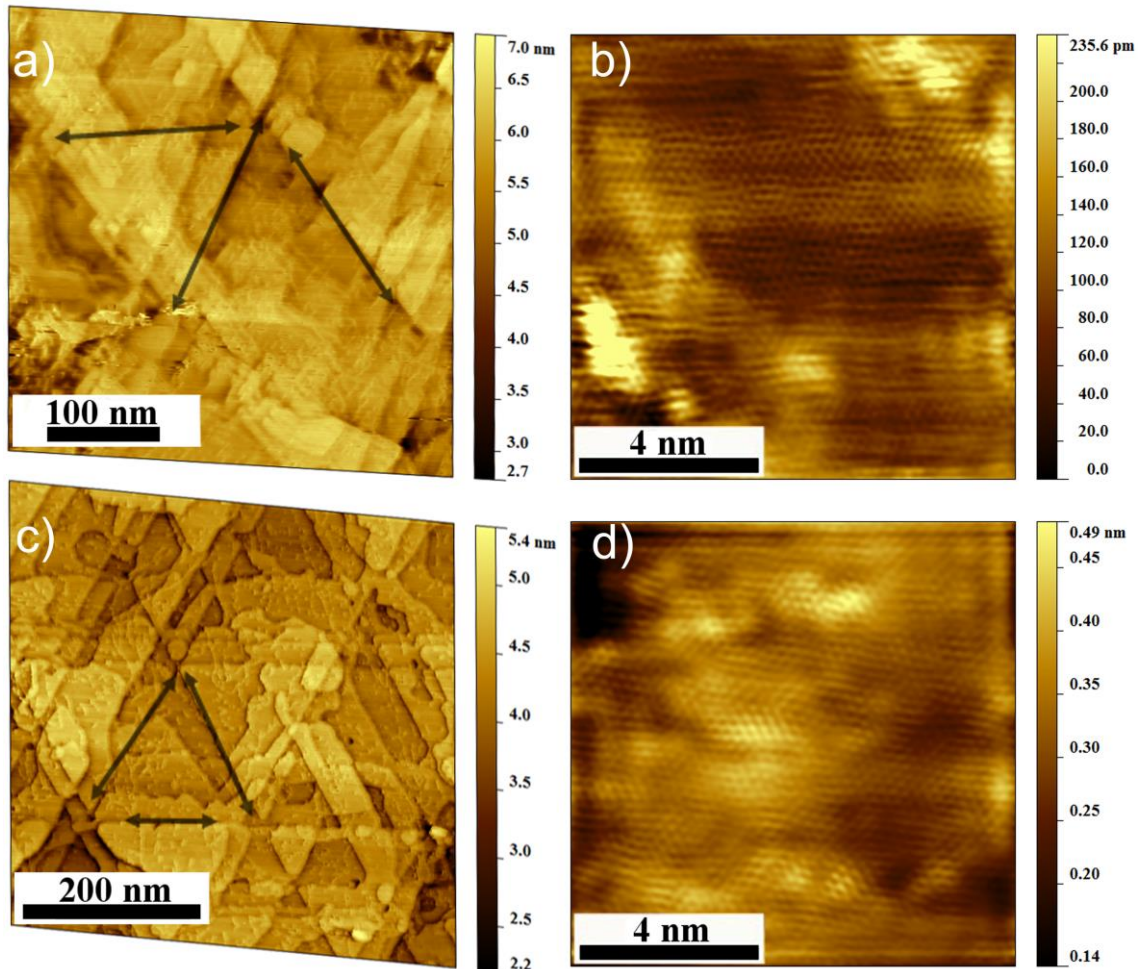
Figure 9. Selected area electron diffraction patterns are presented from different areas of the graphene. The same dominant orientation is present in all of them, as the arrows show in spite of the fact that they were recorded from areas situated far (1 mm) from each other. That fact proves that the graphene layer has the same dominant orientation over an area that is at least 1 mm wide. It is taken as evidence that the graphene grew epitaxially over the Ni (111) surface.
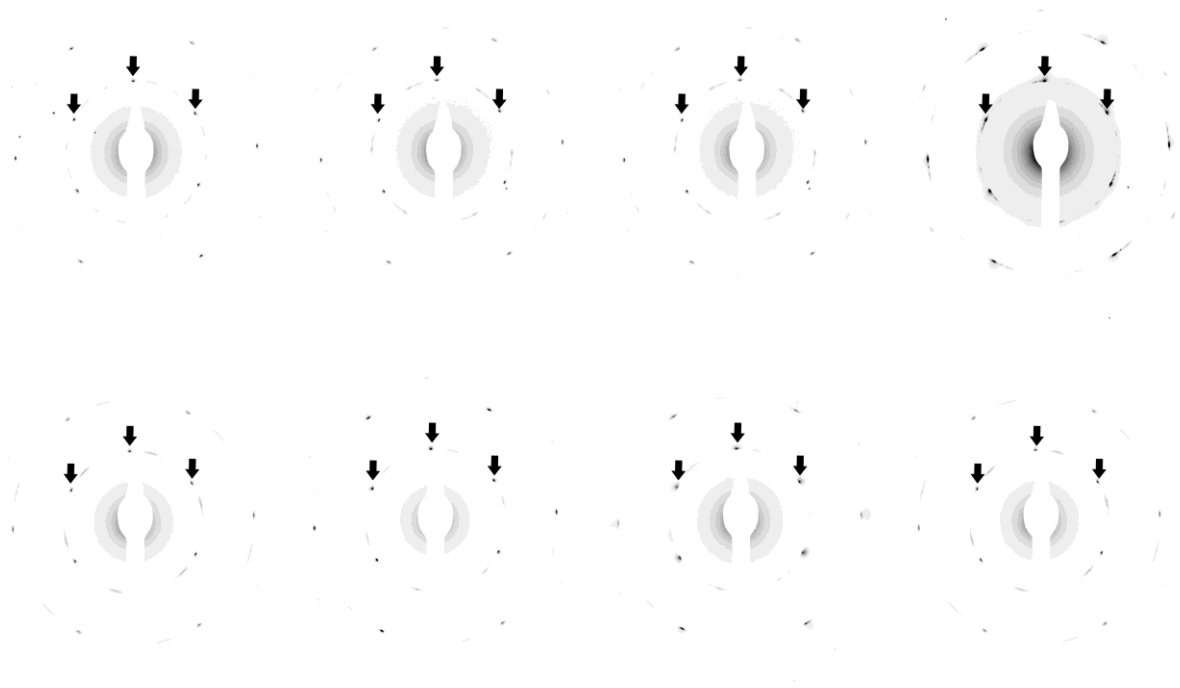

Figure 10. On the left side, a HRTEM image of grain boundaries around a few small grains is seen in the continuously grown graphene. One of them is marked with an arrow. Moiré pattern formed by 10-20 μm wide flakes and the continuously grown graphene is shown on the right side HRTEM image.
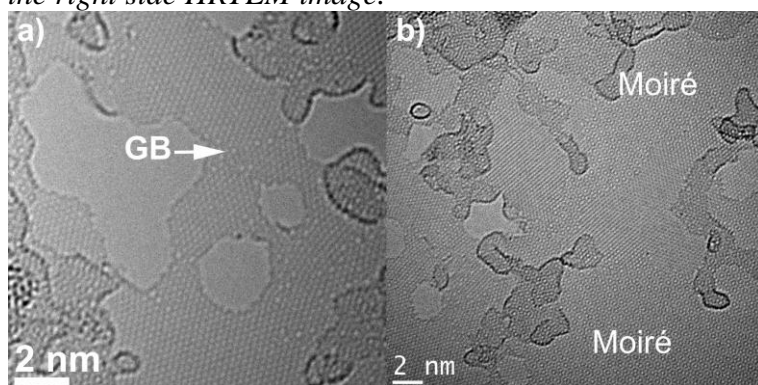
Figure 11. The results of the Raman investigation from "free-standing" graphene are seen. The dotted line is from a carbon support membrane with graphene on top of it and extending over a hole in the membrane. The dashed line is from the amorphous carbon membrane alone. The graphene spectrum was obtained as a difference of the above two spectra (continuous line).